

# Resonant Scattering and Ly $\alpha$ Radiation Emergent from Neutral Hydrogen Halos

Ishani Roy<sup>1</sup>, Chi-Wang Shu<sup>1</sup>, and Li-Zhi Fang<sup>2</sup>

## ABSTRACT

With a state-of-the-art numerical method for solving the integral-differential equation of radiative transfer, we investigate the flux of the Ly $\alpha$  photon emergent from an optical thick halo containing a central light source. Our focus is on the time-dependent effects of the resonant scattering. We first show that the frequency distribution of photons in the halo are quickly approaching to a locally thermalized state around the resonant frequency, even when the mean intensity of the radiation is highly time-dependent. Since initial conditions are forgotten during the thermalization, some features of the flux, such as the two peak structure of its profile, actually are independent of the intrinsic width and time behavior of the central source, if the emergent photons are mainly from photons in the thermalized state. In this case, the difference  $|\nu_{\pm} - \nu_0|$ , where  $\nu_{\pm}$  are the frequencies of the two peaks of the flux, cannot be less than 2 times of Doppler broadening. We then study the radiative transfer in the case where the light emitted from the central source is a flash. We calculate the light curves of the flux from the halo. It shows that the flux is still a flash. The time duration of the flash for the flux, however, is independent of the original time duration of the light source but depends on the optical depth of the halo. Therefore, the spatial transfer of resonant photons is a diffusion process, even though it is not a purely Brownian diffusion. This property enables an optical thick halo to trap and store thermalized photons around  $\nu_0$  for a long time after the cease of the central source emission. The photons trapped in the halo can yield delayed emission, of which the profile also shows typical two peak structure as that from locally thermalized photons. Possible applications of these results are addressed.

*Subject headings:* cosmology: theory - intergalactic medium - radiation transfer - scattering

---

<sup>1</sup>Division of Applied Mathematics, Brown University, Providence, RI 02912

<sup>2</sup>Department of Physics, University of Arizona, Tucson, AZ 85721

## 1. Introduction

The transfer of Ly $\alpha$  radiation in optically thick medium is fundamentally important for the understanding of the physics of halos around Ly $\alpha$  photon sources or clouds nearby these sources. It includes Ly $\alpha$  forest, damped Ly $\alpha$  system, Ly $\alpha$  blob, Ly $\alpha$  emitter and fluorescent Ly $\alpha$  emission of galaxies and quasars, as well as the optical afterglow of gamma ray bursts. The profiles of the emission and absorption of the Ly $\alpha$  radiation from these sources are powerful tools to constrain the mass density, velocity, temperature and the fraction of neutral hydrogen of IGM at various redshifts (Miralda-Escude & Rees 1998; Miralda-Escude 1998; Haiman & Cen 2005; Tasitsiomi 2006; Totani et al. 2006; McQuinn et al. 2007).

It is well known that the resonant scattering of Ly $\alpha$  photons with neutral hydrogen atoms has a profound effect on the time, space and frequency dependencies of the transfer of Ly $\alpha$  photons. An analytical solution of the integro-differential equation of the resonant radiative transfer revealed that the resonant scattering leads to a local Boltzmann distribution of photons in a small frequency range around Ly $\alpha$  frequency  $\nu_0$  (Wouthuysen 1952; Field 1958, 1959). The temperature of the Boltzmann distribution is equal to the kinetic temperature of the neutral hydrogen atoms. The width of the local Boltzmann distribution is increasing with time. This is the so-called Wouthuysen-Field effect, which is important in 21 cm cosmology (Fang 2009).

Besides Field’s solution, no other time-dependent analytical solutions of the integro-differential equation are available. All other analytical solutions (Harrington 1973; Neufeld 1990; Dijkstra et al. 2006) are based on the time-independent Fokker-Planck equation, which is the diffusion approximation of the radiation transfer. These time-independent solutions are important, but can only be used to describe the “limiting asymptotic behavior” of the radiative transfer (Adams 1972). It gives nothing of the time-development of the local Boltzmann distribution. The Monte Carlo numerical method has also been used to solve the radiative transfer of Ly $\alpha$  photons (Lee 1974, Zheng & Miralda-Escude 2002; Ahn 2002; Cantalupo et al. 2005; Verhamme 2006). Yet, the time-development of the Wouthuysen-Field effect is also absent in this approach.

Time-independent approximation would be reasonable if the length scale  $l$  and time scales  $t$  of the problem considered satisfy the condition  $l/t \ll c$ . In this case, one can take  $c \rightarrow \infty$ , and then, the time derivative term  $\partial/c\partial t$  of the radiative transfer equation can be dropped. The condition  $l/t \ll c$ , however, cannot be satisfied if the size of the neutral hydrogen halo is large and the time scale of the Ly $\alpha$  photon source is small. For instance, the time scale  $t_{\text{after}}$  of the optical afterglow of GRBs is of the order of a few tens of hours (e.g. Tanvir et al. 2009; Salvaterra et al. 2009), or a few days (Vreeswijk et al. 2004), while the column number density of neutral hydrogen is as large as  $10^{21-22} \text{ cm}^{-2}$ , and number volume

density is about  $10^2 - 10^4 \text{ cm}^{-3}$  (Vreeswijk et al. 2004). Therefore, the size of the neutral hydrogen halos should be much larger than  $ct_{\text{after}}$ . It is improper to treat the short-time problems with the solutions of “limiting asymptotic behavior”.

Recently, a state-of-the-art numerical solver for the kinetic equations has been developed. This solver is based on the weighted essentially non-oscillatory (WENO) scheme (Jiang & Shu 1996). It has been developed to solve the Boltzmann equations (Carrillo et al. 2003, 2006) and radiative transfer (Qiu et al. 2006, 2007, 2008). This numerical solver has successfully passed the tests of conservation of photon number, Field’s solutions and the Wouthuysen-Field effect etc., and has been properly used as the solver of the transfer of resonant photons (Roy et al. 2009a, b, c).

We will study, in this paper, the time-dependent behavior of the Ly $\alpha$  radiation transfer in an optical thick medium. We will not try to explain any specific observed Ly $\alpha$  spectrum, instead we will study the physical features of the resonant photon transfer, which can not be addressed with previous solvers. For instance, we will show that the frequency distribution of the Ly $\alpha$  photons can keep in a locally thermalized state even when the intensity and flux are highly time-dependent. This feature is essentially important, as thermalization generally will lead to the initial conditions being forgotten. Our solver is also able to study the transfer of a light flash in optical thick halo. It shows that the nature of the transfer is a diffusion process, though it is not a purely Brownian diffusion. This property leads to the trap and store of photons thermalized around the Ly $\alpha$  frequency for a long time after the cease of the central source emission.

This paper is organized as follows. Section 2 presents the theoretical background of the Ly $\alpha$  photon transfer in an optically thick medium. Section 3 gives the solution of Ly $\alpha$  photons emergent from an optical thick spherical halos with a time-independent source located at the center of the halo. Section 4 is on the solutions when the central source is a flash. A discussion and conclusion are given in Section 5. The details of the numerical implementation is given in the Appendix.

## 2. Theory of Ly $\alpha$ radiative transfers in optically thick halos

### 2.1. Optically thick halos

The property of the halo around individual luminous object depends on the luminosity, the spectrum of UV photon emission, and the time-evolution of the center object. For luminous objects at high redshift, the halos generally consist of three spheres (Cen 2006; Liu et al. 2007). The most inner region is the highly ionized Strömngren sphere, or the HII

region, which is optically thin of Ly $\alpha$  photons. The second region, which is just outside the HII region, is optically thick of Ly $\alpha$  photons. The temperature of the baryon gas is about  $10^4$  K, which is due the heating of the UV photons. The third region is outside of the heated region. It is un-heated, and therefore, the temperature of the baryon gas can be as low as  $10^2$  K.

In this context, we will study the transfer of Ly $\alpha$  photons in a radius  $R$  spherical halo of neutral hydrogen with temperature  $T$  in the range of  $10^2$  to  $10^4$  K. Assuming the uniformly distributed HI gas has number density  $n_{\text{HI}}$ , the optical depth over a light path  $dl$  is  $d\tau(\nu) = n_{\text{HI}}dl$ .  $\sigma(\nu)$  is the cross section of the resonant scattering of Ly $\alpha$  photons by hydrogen, given as

$$\sigma(x) = \sigma_0(\Delta\nu_D)^{-1}\phi(x, a) \quad (1)$$

where  $x$  is the dimensionless frequency defined by  $x \equiv (\nu - \nu_0)/\Delta\nu_D$ ,  $\nu_0$  being the resonant frequency.  $\Delta\nu_D = \nu_0(v_T/c)$  is the Doppler broadening, and  $v_T = \sqrt{2k_B T/m}$ . Therefore,  $x$  measures the frequency deviation  $\Delta\nu = |\nu - \nu_0|$  in units of  $\Delta\nu_D = 1.06 \times 10^{11}(T/10^4)^{1/2}$  Hz.  $\sigma_0 = \pi e^2 f/m_e c = 1.10 \times 10^{-2}$  cm<sup>2</sup> is the cross section of the resonant scattering at frequency  $\nu_0 = 2.46 \times 10^{15}$  s<sup>-1</sup>. The function  $\phi(x, a)$  in equation (1) is the normalized profile given by the Voigt function as (Hummer 1965)

$$\phi(x, a) = \frac{a}{\pi^{3/2}} \int_{-\infty}^{\infty} dy \frac{e^{-y^2}}{(x-y)^2 + a^2}. \quad (2)$$

The parameter  $a$  in equation (2) is the ratio of the natural to the Doppler broadening. For the Ly $\alpha$  line,  $a = 2.35 \times 10^{-4}(T/10^4)^{-1/2}$ . The optical depth of the halo with column number density of neutral hydrogen  $N_{\text{HI}} = n_{\text{HI}}R$  is

$$\tau(x) = N_{\text{HI}}\sigma(x) = \tau_0\phi(x), \quad (3)$$

where

$$\tau_0 = N_{\text{HI}}\sigma_0(\Delta\nu_D)^{-1} = 1.04 \times 10^7 \left(\frac{T}{10^4}\right)^{-1/2} \left(\frac{N_{\text{HI}}}{10^{20}\text{cm}^2}\right). \quad (4)$$

## 2.2. Radiative transfer equation in spherical halo

The radiative transfer of Ly $\alpha$  photons in spherical halo is described by the equation of the specific intensity  $I(\eta, r, x, \mu)$  as

$$\begin{aligned} \frac{\partial I}{\partial \eta} + \mu \frac{\partial I}{\partial r} + \frac{(1 - \mu^2)}{r} \frac{\partial I}{\partial \mu} - \gamma \frac{\partial I}{\partial x} = \\ -\phi(x; a)I + \int \mathcal{R}(x, x'; a)I(\eta, r, x', \mu')dx'd\mu' + S, \end{aligned} \quad (5)$$

where we use dimensionless time  $\eta$  defined as  $\eta = cn_{\text{HI}}\sigma_0(\Delta\nu_D)^{-1}t$  and dimensionless coordinate  $r$  defined as  $r = n_{\text{HI}}\sigma_0(\Delta\nu_D)^{-1}r_p$ , with  $r_p$  being the physical radial coordinate. That is,  $\eta$  and  $r$  are, respectively, in the units of mean free flight-time and mean free path of photon  $\nu_0$ . For a signal propagated in the radial direction with the speed of light, we have  $r = \eta + \text{const}$ . In equation (5)  $\mu = \cos\theta$  is the direction relative to the radial vector  $\mathbf{r}$ .

The re-distribution function  $\mathcal{R}(x, x'; a)$  gives the probability of a photon absorbed at the frequency  $x'$ , and re-emitted at the frequency  $x$ . It depends on the details of the scattering (Henyey 1941; Hummer 1962; Hummer 1969). If we consider coherent scattering without recoil, the re-distribution function with the Voigt profile equation (2) is

$$\mathcal{R}(x, x'; a) = \frac{1}{\pi^{3/2}} \int_{|x-x'|/2}^{\infty} e^{-u^2} \left[ \tan^{-1} \left( \frac{x_{\min} + u}{a} \right) - \tan^{-1} \left( \frac{x_{\max} - u}{a} \right) \right] du \quad (6)$$

where  $x_{\min} = \min(x, x')$  and  $x_{\max} = \max(x, x')$ . In the case of  $a = 0$ , i.e. considering only the Doppler broadening, the re-distribution function is

$$\mathcal{R}(x, x') = \frac{1}{2} \text{erfc}[\max(|x|, |x'|)]. \quad (7)$$

The re-distribution function of equation (7) is normalized as  $\int_{-\infty}^{\infty} \mathcal{R}(x, x') dx' = \phi(x, 0) = \pi^{-1/2} e^{-x^2}$ . With this normalization, the total number of photons is conserved in the evolution described by equation (5). That is, the destruction processes of Ly $\alpha$  photons, such as the two-photon process (Spitzer & Greenstein 1951; Osterbrock 1962), is ignored in Equation (5). In equations (6) and (7), we also do not consider the recoil of atoms. It is equal to assume the mass of atom is very large. The effect of recoil actually is under control (Roy et al. 2009c). We will address it in next section.

In equation (5), the term with the parameter  $\gamma$  is due to the expansion of the universe. If  $n_{\text{H}}$  is equal to the mean of the number density of cosmic hydrogen, we have  $\gamma = \tau_{\text{GP}}^{-1}$ , and  $\tau_{\text{GP}}$  is the Gunn-Peterson optical depth. Since Gunn-Peterson optical depth is of the order of  $10^6$  at high redshift (e.g. Roy et al. 2009c), we will take the parameter  $\gamma = 10^{-5} - 10^{-6}$ .

### 2.3. Eddington approximation

When the optical depth is large, we can take the Eddington approximation as

$$I(\eta, r, x, \mu) \simeq J(\eta, r, x) + 3\mu F(\eta, r, x) \quad (8)$$

where  $J(\eta, r, x) = \frac{1}{2} \int_{-1}^{+1} I(\eta, r, x, \mu) d\mu$  is the angularly averaged specific intensity and  $F(\eta, r, x) = \frac{1}{2} \int_{-1}^{+1} \mu I(\eta, r, x, \mu) d\mu$  is the flux. Defining  $j = r^2 J$  and  $f = r^2 F$ , Eq. (5) yields the equations

of  $j$  and  $f$  as

$$\frac{\partial j}{\partial \eta} + \frac{\partial f}{\partial r} = -\phi(x; a)j + \int \mathcal{R}(x, x'; a)j dx' + \gamma \frac{\partial j}{\partial x} + r^2 S, \quad (9)$$

$$\frac{\partial f}{\partial \eta} + \frac{1}{3} \frac{\partial j}{\partial r} - \frac{2j}{3r} = -\phi(x; a)f. \quad (10)$$

The mean intensity  $j(\eta, r, x)$  describes the  $x$  photons trapped in the halo by the resonant scattering, while the flux  $f(\eta, r, x)$  describes the photons in transit.

Without resonant scattering, equations (9) and (10) give

$$\frac{\partial j}{\partial \eta} + \frac{\partial f}{\partial r} = -\phi(x; a)j + \gamma \frac{\partial j}{\partial x} + r^2 S, \quad (11)$$

$$\frac{\partial f}{\partial \eta} + \frac{1}{3} \frac{\partial j}{\partial r} - \frac{2j}{3r} = -\phi(x; a)f. \quad (12)$$

For photons with frequency shifted away from  $\nu_0$ , the halo would be optically thin, and therefore, the Eddington approximation will no longer be proper when the variable  $x$  is large. However we are mainly interested in the profile around  $x = 0$ , hence the Eddington approximation is available.

The source term  $S$  in the equations (9) and (11) can be described by a boundary condition of  $j$  and  $f$  at  $r = r_0$ . We can take  $r_0 = 0$ , as  $r_0$  is not important if the optical depth of the halo is large. Thus, we have

$$j(\eta, 0, x) = 0, \quad f(\eta, 0, x) = S_0 \phi_s(x), \quad (13)$$

where  $S_0$ , and  $\phi_s(x)$  are, respectively, the intensity and normalized frequency profile of the sources. Since equation (9)-(12) are linear, the intensity  $S_0$  can be taken as any constant. That is, the solution  $f(x)$  of  $S_0 = S$  is equal to  $S f_1(x)$ , where  $f_1(x)$  is the solution of  $S = 1$ . On the other hand, the equations (9) and (10) are not linear with respect to the function  $\phi_s(x)$ , i.e. the solution  $f(x)$  of  $\phi_s(x)$  is not equal to  $\phi_s(x) f_1(x)$ , where  $f_1$  is the solution of  $\phi_s(x) = 1$ .

In the range outside the halo,  $r > R$ , no photons propagate in the direction  $\mu < 0$ . Therefore, the boundary condition at  $r = R$  given by  $\int_0^{-1} \mu J(\eta, R, x, \mu) d\mu = 0$  is then (Unno 1955)

$$j(\eta, R, x) = 2f(\eta, R, x). \quad (14)$$

There is no photon in the field before  $t = 0$ . Therefore, the initial condition is

$$j(0, r, x) = f(0, r, x) = 0. \quad (15)$$

We solve equations (9) and (10) or equations (11) and (12) with the numerical method developed recently (Roy et al. 2009a, 2009b, 2009c). Some details of this method is given in the Appendix. We first solve the problems when the sources  $S$  are time-independent.

### 3. Solutions of time-independent sources

#### 3.1. Time scale of local thermalization

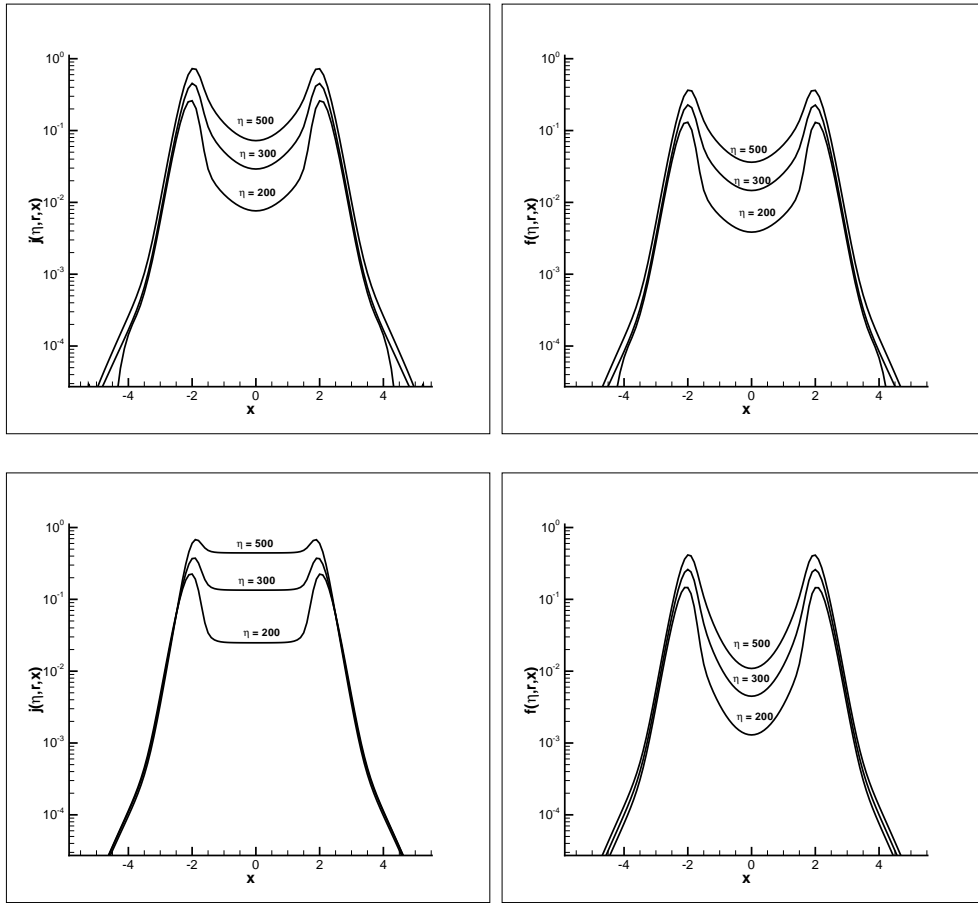


Fig. 1.— Top two panels are the solutions of  $j(\eta, r, x)$  (left) and  $f(\eta, r, x)$  (right) of equations (9) and (10) at  $r = R = 10^2$  and  $\eta = 200, 300, 500$  with the boundary condition equation (14). Bottom two panels are the solutions without the boundary condition equation (14). The source is  $S_0 = 1$  and  $\phi_s(x) = (1/\sqrt{\pi})e^{-x^2}$ . The parameters are taken to be  $a = 10^{-3}$  and  $\gamma = 0^{-5}$ .

A typical time-dependent solution of the mean intensity  $j(\eta, r, x)$  and flux  $f(\eta, r, x)$  is shown in Figure 1. The top two panels are the solutions of  $j(\eta, r, x)$  (left) and  $f(\eta, r, x)$  (right) of equations (9) and (10) at radius  $r = 10^2$  and time  $\eta = 200, 300, 500$  with the boundary condition equations (13) and (14). The bottom two panels are the solutions without the boundary condition equation (14) at  $R$ . The parameters  $a$  and  $\gamma$  are taken to be  $10^{-3}$  and  $10^{-5}$ , respectively. The effect of  $\gamma = 10^{-5}$  actually is ignorable in these solutions. The source constant is taken to be  $S_0 = 1$  and the normalized line profile is  $\phi_s(x) = (1/\sqrt{\pi})e^{-x^2}$ , i.e. the emission line width is equal to the Doppler broadening, and total luminosity of the source is  $\int S_0\phi_s(x)dx = 1$ .

If Ly $\alpha$  photon transfer is due only to spatial diffusion, the time scale of a spatial transfer with optical depth  $\tau_0 = 10^2$  should be as large as  $\eta \sim \tau_0^2 = 10^4$ . However, Figure 1 shows that  $\int f(\eta, r, x)dx \sim 1$  at  $r = 10^2$  and  $\eta = 500$ . It means that photons have already escaped from the  $\tau_0 = 10^2$  hole within the time  $\eta \sim 500$ , which is much less than the time scale of a purely spatial diffusion. Therefore, Figure 1 indicates that the photon’s transfer should not be a process of purely Brownian diffusion. This point is very well known in early studies on the escape of resonant photon from opaque clouds (Osterbrock 1962; Harrington 1973; Avery & House 1968). However, these works are mainly based on the time scale of the escape of photons with frequency, which can take a “single longest excursion” (Adams 1972). Figure 1 shows that the time scale  $\eta = 500$  is true not only for photons which can take a “single longest excursion”, but also for all photons with frequency around  $\nu_0$  or  $x = 0$ .

The solution  $f$  in the right bottom panel is about the same as that in the top panel. That is, the flux is almost independent of the boundary condition equation (14). This point has been noted for the static solutions of equations (9) and (10) (Unno 1955; Neufeld 1990). This is because in optical thick medium, photons cannot feel the boundary even at a position  $r$  very close to the boundary. On the other hand, the last scattering of escaped photons should be dominated by the scattering at the position very close to the boundary. Therefore, in terms of calculating  $f$ , the boundary condition equation (14) is not important.

However, the solution  $j$  of the bottom left panel in Figure 1 shows a flat plateau around  $x = 0$ , while the solution  $j$  of the top left panel of Figure 1 does not show such flat plateau. As has been shown (Roy et al. 2009c), the flat plateau actually is the Boltzmann statistical equilibrium distribution around  $x = 0$  if the atomic mass is infinite. If the mass is finite, i.e. considering the recoil in the re-distribution functions (6) or (7), the flat plateau will become  $e^{-2bx}$ , where  $b = h\nu_0/mv_{Tc}$ . This is the local Boltzmann distribution required by the Wouthuysen-Field effect (Roy et al. 2009b). Therefore, the solution  $j$  at the bottom left of Figure 1 shows that at position close to the boundary the frequency distribution of photons is of local statistical equilibrium or thermalized around  $x = 0$ . On the other hand,

photons at the boundary  $R$  have not taken enough number of scattering before escaping from the halo, and therefore, they are not thermalized.

In the time range from  $\eta = 200$  to 500, the mean intensity  $j$  at  $x = 0$  quickly increases by a factor larger than 10. However, the flat plateau or the local thermalization around  $x = 0$  is perfectly held during the fast evolution of the intensity  $j$ . This result is important. The photons of the flux  $f$  around  $x = 0$  emergent from the boundary  $R$  of optical thick halo mostly come from the photons at a position close to the boundary. Thus, the immediate source of the flux  $f$  actually is thermalized, regardless of the initial distribution of the photons. The initial conditions of photon source have already been forgotten during the thermalization. Therefore, one can expect that some properties of the flux  $f$  have to be independent of the sources.

### 3.2. Restoring $\nu_0$ photons

Figure 1 shows that the flux has a valley at  $x = 0$ , while the mean intensity  $j$  at time  $\eta = 500$  has a rather high amount at  $x = 0$ . This indicates that  $\nu_0$  photons are restored by the resonant scattering. According to the re-distribution function  $\mathcal{R}(x, x')$  equation (5), the probability of transferring a  $x'$  photon to a  $|x| < |x'|$  photon is larger than that from  $x'$  to  $|x| > |x'|$ . Therefore, the net effect of resonant scattering is to bring photons with frequency  $x' \neq 0$  to the central range  $x \sim 0$  of frequency space. Photons of  $x \sim 0$  are then effectively restored. The top right panel of Figure 1 shows that at  $\eta = 500$  the flux  $f$  at  $x = 0$  can be as large as about 1/10 of the flux at its two peaks of  $x \simeq \pm(2 - 3)$  which would be observable.

As a comparison to Figure 1, we solve the mean intensity  $j(\eta, r, x)$  and flux  $f(\eta, r, x)$  with equations (11) and (12). The result is shown in Figure 2, of which the parameters are the same as those in Figure 1. Both  $j$  or  $f$  in Figure 2 are very different from that in Figure 1. The profiles in Figure 2 typically are an absorption spectrum, which has a very deep valley at  $x = 0$ . The absorption of  $\nu_0$  photons at  $r = 10^2$  (or  $\tau_0 = 10^2$ ) is  $e^{-100} = 10^{-43}$ , which is the amount of  $j$  and  $f$  shown in Figure 2.

The curves in Figure 2 do not show any evolution in the time range  $\eta = 200 - 500$ . It means that  $j$  and  $f$  at the radius  $r = 10^2$  have already been stable at the time  $\eta < 200$ . Therefore, the time-evolution of  $j$  and  $f$  after  $\eta = 200$  shown in Figure 1 is fully caused by the resonant scattering. The thermalization and the restoration of  $\nu_0$  photons are from this delayed evolution.

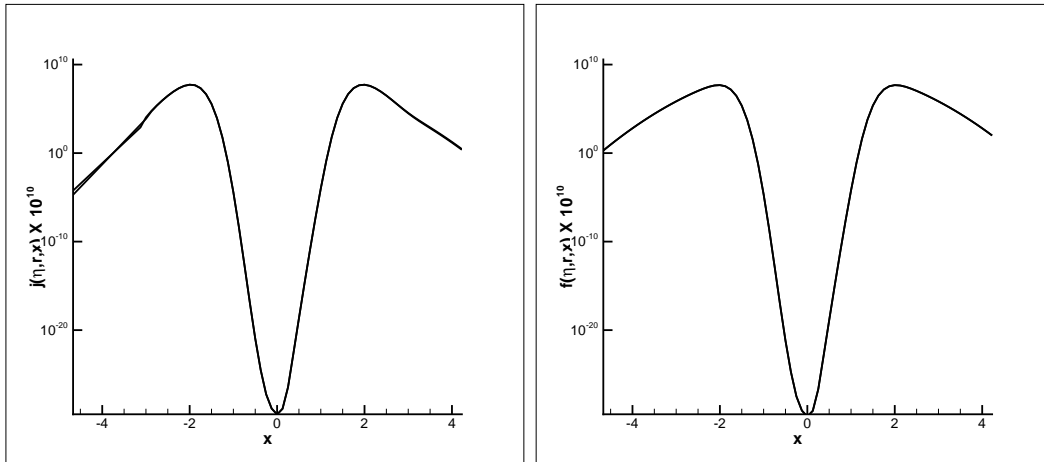


Fig. 2.— Solutions of  $j(\eta, r, x)$  (left) and  $f(\eta, r, x)$  (right) of eqs. (11) and (12) at  $r = 10^2$  and  $\eta = 200, 300, 500$ . The source and all parameters are the same as in Figure 1.

### 3.3. Two peaks in the flux profile

The profiles of both  $j$  and  $f$  shown in Figure 1 have two peak structure. The flux  $f$  is dominated by photons with frequency  $x_{\pm} \simeq \pm(2 - 3)$ . The two peak structure has been recognized in all the time-independent solutions of the Fokker-Planck approximation (Harrington 1973; Neufeld 1990; Dijkstra et al. 2006), and Monte Carlo simulation (Lee 1974; Zheng & Miralda-Escude 2002; Ahn et al. 2002; Cantalupo et al. 2005; Verhamme et al. 2006). What a point we want to emphasize is that this structure is independent of the profile of the source  $S$ . It is because the initial properties of the central sources have been forgotten during the local thermalization.

Figure 3 presents the flux  $f$  given by equations (9) and (10) with the same parameters as the solution shown Figure 1, and the source profile  $\phi_s(x) = (1/\sqrt{\pi})e^{-x^2}$  replaced by  $\phi_s(x) = (1/\sqrt{\pi/2})e^{-2x^2}$ . That is, the line width of the new one is equal to 1/2 of that in Figure 1. Figure 3 plots the solution of  $f$ , which is identical with the bottom-right panel of Figure 1. It shows that the initial distribution of photon frequency is already forgotten, and therefore, the flux of Figures 1 and 2 at  $\eta > 200$  actually are from the same thermalized sources. The flux of Figures 1 and 2 are also held if the line width is broader than  $\phi_s(x) = (1/\sqrt{\pi})e^{-x^2}$ . We will show this even when the source has a continuant spectrum (§3.4).

Since the shape of the local thermalized distribution is time-independent, the frequency of the two peaks,  $|x_{\pm}|$ , at a given  $r$  is also time-independent. When the photons of the flux  $f$

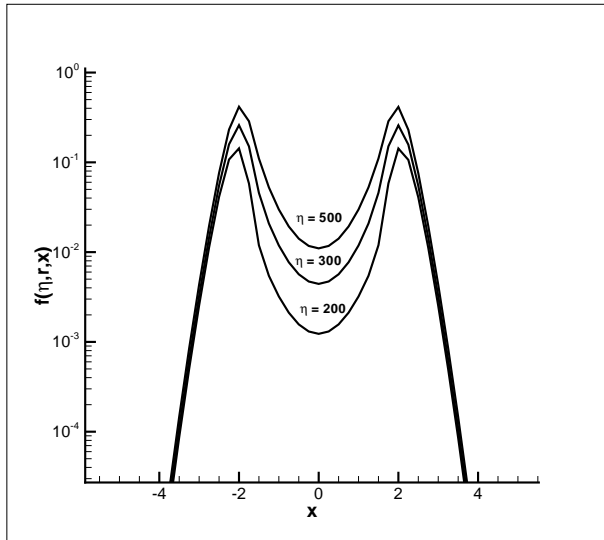


Fig. 3.— Flux  $f(\eta, r, x)$  at radius  $r = 10^2$  and time  $\eta = 200, 300$  and  $500$ . The frequency profile of the source is  $\phi_s(x) = (1/\sqrt{\pi/2})e^{-2x^2}$ . Other parameters are the same as in Figure 1

mainly come from the local thermalized photons, the frequency of the two peaks,  $|x_{\pm}|$ , should not be described by the relation  $|x_{\pm}| = (a\tau)^{1/3}$ , because this relation is from a solution of the time-independent Fokker-Planck equation, which does not describe the thermalization (Neufeld 1990).

Figure 4 presents the peak frequency  $|x_{\pm}|$  as a function of  $ar$  for solutions given by equations (9) and (10) with  $a = 10^{-2}$ . We consider only  $r \geq 10^2$ , as in the case  $r \leq 10^2$  photons do not undergo a large enough number of scattering, and therefore, are not completely thermalized yet. With the dimensionless variables,  $ar$  is equal to  $a\tau$ . A line  $|x_{\pm}| = (ar)^{1/3}$  is also shown in Figure 4. It shows that our numerical result of  $|x_{\pm}|$  is significantly different from the  $(a\tau_0)^{1/3}$ -law if  $ar < 30$ . That is, in the range  $ar < 30$ , photons of the flux  $f$  are dominated by the local thermalized photons. The frequency  $x_{\pm}$  actually is dependent on the width of the flat plateau or the local thermalized distribution of  $j$ . Therefore,  $x_{\pm}$  is always larger than two. The curve of Figure 4 is approximately available for  $a = 10^{-3}$  and  $10^{-4}$ . Thus,  $|x_{\pm}|$  is larger than  $(ar)^{1/3}$  if  $r < 3 \times 10^5$  and  $3 \times 10^6$  for  $a = 10^{-3}$  and  $10^{-4}$ , respectively.

Figure 4 shows a slowly increase of  $|x_{\pm}|$  with  $r$  in the range  $ar \leq 30$ , and then, it approaches  $(ar)^{1/3}$  for larger  $ar$ . When  $r$  is large, more photons of the flux are attributed to the resonant scattering by the Lorentzian wing of the Voigt function.  $|x_{\pm}|$  is then approaching

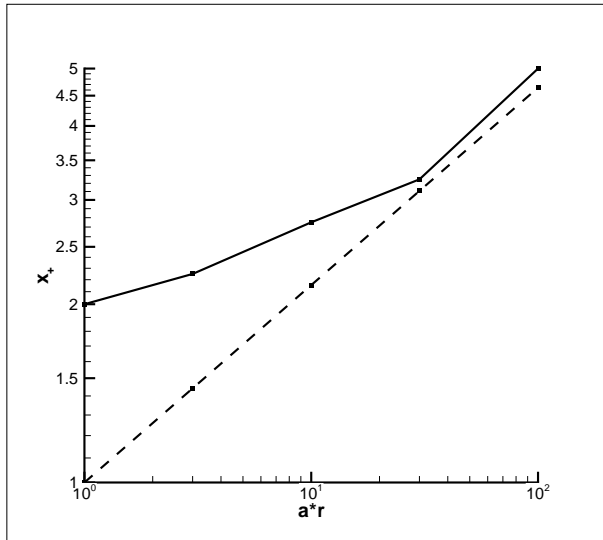


Fig. 4.— The positions of the peaks  $|x_+|$  as a function of  $(ar)^{1/3}$  for the solutions of eqs. (9) and (10) with  $a = 10^{-2}$ . Other parameters are the same as in Figure 1. The dashed line is for  $x_{\pm} = \pm(ar)^{1/3}$ .

to  $(ar)^{1/3}$ . It should be emphasized once again that all these results are independent of the intrinsic width of Ly $\alpha$  emission from the central source.

### 3.4. Absorption spectrum

If the radiation from the sources has continuum spectrum, the effect of neutral hydrogen halos is to produce an absorption line at  $\nu = \nu_0$ . The profile of the absorption line can also be found by solving equations (9) and (10), but replacing the boundary equation (13) by

$$j(\eta, 0, x) = 0, \quad f(\eta, 0, x) = S_0. \quad (16)$$

That is, we assume that the original spectrum is flat in the frequency space.

A solution of the time evolution of  $j$  and  $f$  at  $r = 10^2$  with the source equation (16) is shown in Figure 5. The optical depths at the frequency  $|x| > 4$  are small, and therefore, the Eddington approximation would no longer be proper. However, those photons do not strongly involve the resonant scattering, and hence they do not significantly affect the solution around  $x = 0$ . Therefore, the solution is still useful to study the profiles of  $j$  and  $f$  around  $x = 0$ . The profile of  $f$  typically is an absorption line with width given by the position of the two peak structure. As expected, the profile in the range  $|x| < 4$  is the

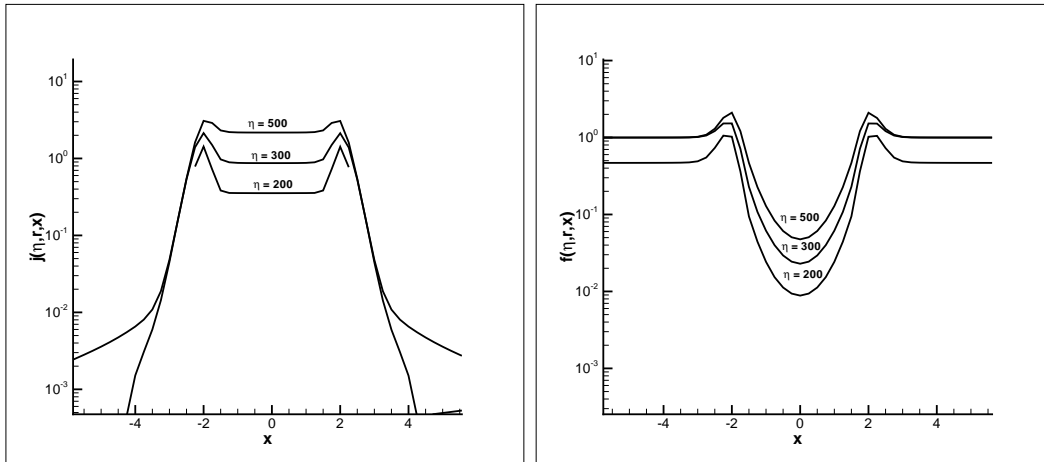


Fig. 5.— Solutions of  $j(\eta, r, x)$  (left) and  $f(\eta, r, x)$  (right) of eqs. (9) and (10) at  $r = 10^2$  and  $\eta = 200, 300$  and  $500$ . The source is given by eq. (16). The parameters are  $a = 10^{-3}$  and  $\gamma = 10^{-5}$ .

same as the bottom right panel of Figure 1. It shows again that the two peak structure is independent of the frequency spectrum of the central source.

The flux  $f$  of Figure 5 has a flat wing in both sides of  $x > 3$  and  $x < -3$ , because the effect of resonant scattering is negligible for photons with frequency  $|x| > 4$ , and they can freely transfer from  $r = 0$  to  $10^2$ . On the other hand, the mean intensity  $j$  does not have wings at  $|x| > 4$ . That is, photons with  $|x| > 4$  cannot be stored in the halo with  $r = 10^2$  at time  $\eta > 200$ . Nevertheless, the intensity  $j$  still has flat plateau around  $x = 0$ . It means that in the period from  $\eta = 200$  to  $\eta = 500$ , the halo trapped and stored more and more photons of  $|x| < 4$ . These photons are in the locally thermalized state.

### 3.5. The estimation of the HI column density

As an application of the absorption spectrum in Figure 5, we study the profile of the red damping wing of the optically thick IGM at high redshifts. Since the variable  $x$  is independent of redshift, the profile of a red damping wing is directly given by the flux  $f(\eta, r, x)$  at the wing of low frequency  $x \leq 0$ .

Red damping wing is sometimes modeled with a damped Ly $\alpha$  system (DLA), which assumes that the damping wing profile is fully determined by the absorption of an optical thick halos around the host objects. The DLA profile of a red damping wing is then given

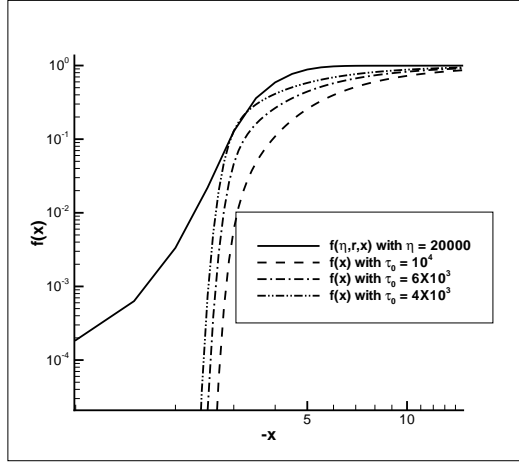


Fig. 6.— Red damping wing (a) the DLA model  $\tau_0 = 4 \times 10^3$  (dotdot dashed line),  $6 \times 10^3$  (dot dashed line) and  $10^4$  (dashed line); (b) the solution  $f(x)$  of §3.4 for  $\tau_0 = 10^4$  (solid line). For both (a) and (b), the parameter  $a = 10^{-2}$ .

by  $f(x) = e^{-\tau(x)}$  and  $x < 0$ , where  $\tau(x)$  is from the Voigt function equation (2) as

$$\tau(x) = \tau_0 \phi(x, a) = \tau_0 \frac{a}{\pi^{3/2}} \int_{-\infty}^{\infty} dy \frac{e^{-y^2}}{(y-x)^2 + a^2}. \quad (17)$$

The column number density of neutral hydrogen atoms,  $N_{\text{HI}}$ , generally is estimated with fitting profile equation (17) with observation, and then,  $N_{\text{HI}}$  can be found from  $\tau_0$  by equation (4).

However, in the optical thick case, we have to consider the effect of resonant scattering. Because resonant scattering helps the transfer of resonant photons, one can expect that the column number density estimated by a fitting of equation (17) should be less than the result when resonant scattering is taken into consideration.

As an example Figure 6 gives a comparison of (a) the red damping wings of eq.(17) with  $\tau_0 = 4 \times 10^3$ ,  $6 \times 10^3$  and  $10^4$ , and (b) a solution  $f$  of §3.4 at  $r = 10^4$ , or  $\tau_0 = 10^4$ . The profiles of (a) and (b) are very different from each other. The former is quickly dropping when  $|x|$  is less than about 3, while the later at  $|x| < 3$  is softly dependent on  $x$ . The curve of (b) approaches to a much higher bottom at  $x = 0$ .

Figure 6 shows that the red damping wing (b) with  $\tau_0 = 10^4$  is always on the left side of (a) having the same optical depth  $\tau_0 = 10^4$ , because resonant scattering makes spatial transfer easier. The curve (a) with  $\tau_0 = 4 \times 10^3$  is more or less close to the curve (b). That is, the DLA model at  $\tau_0 = 4 \times 10^3$  may give a similar data fitting as the solution with

resonant scattering. Therefore, for optical depth  $\tau_0 = 10^4$ , the DLA model of equation (17) will underestimate the column number density of neutral hydrogen by, at least, a factor of 2.

## 4. Solution of flash sources

### 4.1. Frequency-dependence of Ly $\alpha$ transfer

If the light source is significantly time-dependent, like the optical afterglow of GRBs, we can treat the source as a flash described by a boundary conditions as:

$$j(\eta, 0, x) = 0, \quad f(\eta, 0, x) = \begin{cases} S_0 \phi_s(x), & 0 < \eta < \eta_0 \\ 0, & \eta > \eta_0. \end{cases} \quad (18)$$

It describes a flash within a time range  $0 < \eta < \eta_0$ , or the time duration is  $\Delta\eta = \eta_0$ . We consider the case of  $r \geq \eta_0$ . That is, the size of the halo is larger than the spatial range lasted by the flash, as photon spatial transfer in optical thick medium cannot be faster than the speed of light. The initial condition is still the same equation (13).

Figure 7 presents two time-dependent solutions of the mean intensity  $j$  and flux  $f$ : one is for a flash equation (18) with  $\eta_0 = 100$  at  $r = 10^2$ ; the other is for a flash with  $\eta_0 = 500$  at  $r = 10^3$ . Other parameters are  $S_0 = 1$ ,  $a = 10^{-2}$  and  $\phi_s(x) = (1/\sqrt{\pi}) e^{-x^2}$ . We still see the typical flat plateau of  $j$  in all times, even when the original time duration of the flash is as short as  $\Delta\eta = 100$ .

The time dependence of  $j$  has a rising phase and a decaying phase. The thermalization of  $j$  is held in both rising and decaying phases. We see from Figure 7 that the rising and decaying phases are frequency-dependent. Photons at the two peaks reach their maximum at about  $\eta = 200$  (top right panel) and  $\eta = 4000$  (bottom right panel), while the flat plateau reaches their maximum at about  $\eta = 500$  (top right panel) and  $\eta = 6000$  (bottom right panel). That is, the halo holds a local thermalized photons for a much longer time than than the original time durations  $\Delta\eta = 100$  (top) and  $\Delta\eta = 500$  (bottom).

The time-evolution of  $f$  also consists of a rising phase and a decaying phase. Therefore, the flux emergent from the halo is also a flash. However, the time duration is very different from the original one. For the top panel, we see that the profile of  $f$  is almost time-independent from  $\eta = 300$  to 500. That is, the time duration  $500 - 300 = 200$  is much larger than the original one  $\Delta\eta = 100$ . For the bottom panel, the time-independent flux is from  $\eta = 3000$  to 5000, and therefore, the time duration of the flash is about 2000, which is also much larger than the original time duration  $\eta = 500$ .

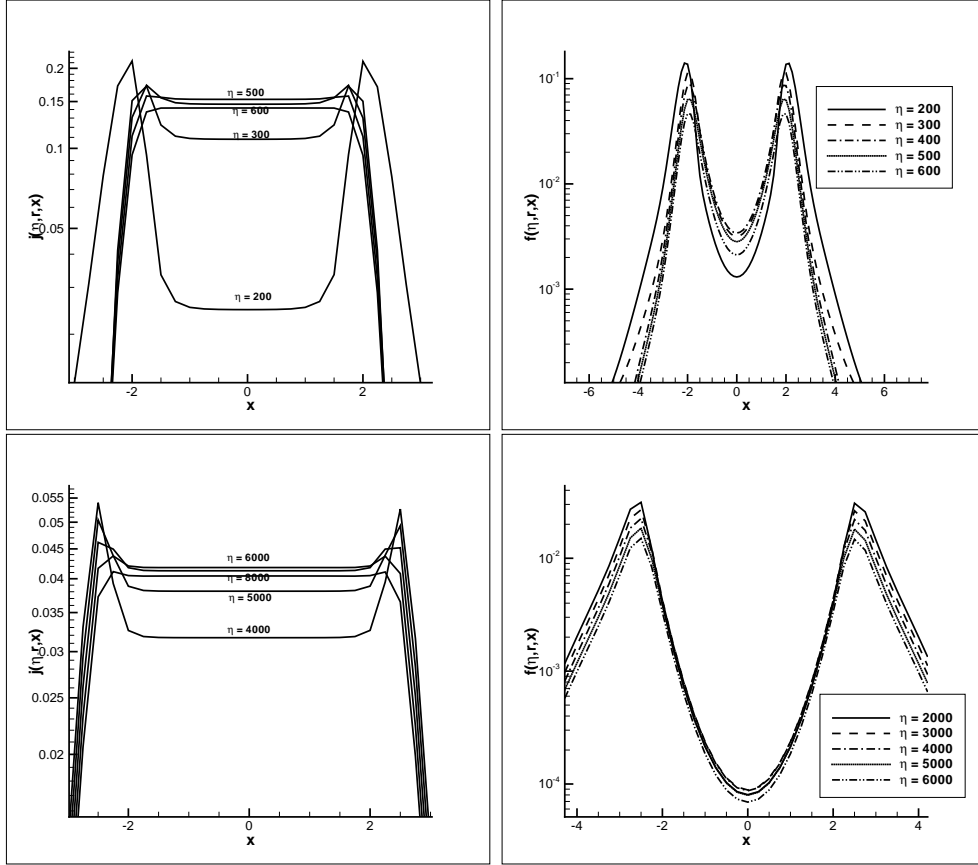


Fig. 7.— The profiles of  $j(\eta, r, x)$  and  $f(\eta, r, x)$  with time-dependent source [eq.(16)]. Top panel:  $j(\eta, r, x)$  (left) and  $f(\eta, r, x)$  (right) of  $\eta_0 = 100$  at  $r = 10^2$ . Bottom panel:  $\eta_0 = 500$  at  $r = 10^3$ . The parameters  $a = 10^{-2}$  and  $\gamma = 10^{-5}$ .

#### 4.2. The evolution of time duration of a flash

To further study the time duration, we plot Figure 8, which gives the light curve, or the time-dependence of the flux  $f$  at  $x = 0$ . It shows the light curve of rising and decaying phases of the flux  $f$ . With these light curves, one can find the maximum of the flux  $f$  at time  $\eta_{max}$ ; the rising phase is then  $\eta < \eta_{max}$ , and decaying phase is  $\eta > \eta_{max}$ . For each curve, one can also define a time duration  $\Delta\eta = \eta_2 - \eta_1$ , where  $\eta_1 < \eta_{max}$  and  $\eta_2 > \eta_{max}$ , and both are given by the condition  $f(\eta_{1,2}, r, 0) = 0.9f(\eta_{max}, r, 0)$ . The time duration is then  $\Delta\eta = \eta_2 - \eta_1$ .

The two top panels of Figure 8 are for a flash source with original time duration  $\Delta\eta = 50$ . Figure 8 shows that the time duration of the flash,  $\Delta\eta$ , is  $r$ -dependent. At  $r = 0$ , i.e. at the

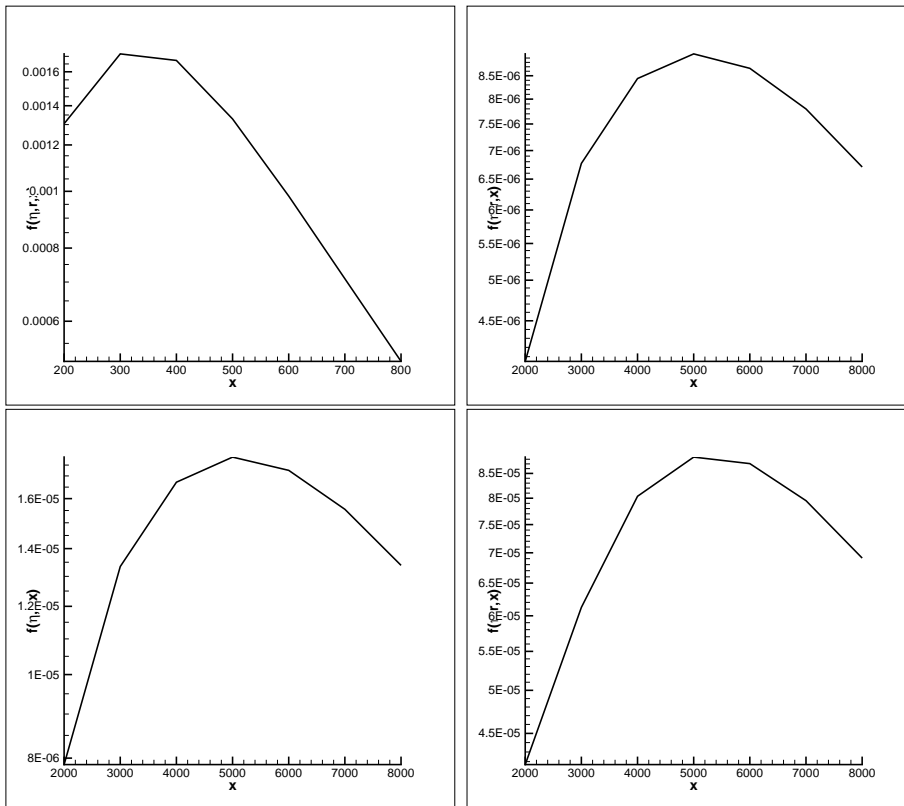


Fig. 8.— The time-dependence of  $f(\eta, r, x)$  at  $x = 0$ . Top panels:  $f(\eta, r, 0)$  at  $r = 10^2$ (left) and  $r = 10^3$ (right) for flash source with  $\eta_0 = 50$ . Bottom panel:  $f(\eta, r, 0)$  at  $r = 10^3$  of flash source with  $\eta_0 = 100$  (left) and  $\eta_0 = 500$ (right).

source,  $\Delta\eta$  is 50. At  $r = 10^2$  (top left of Figure 8),  $\Delta\eta$  is about 200, while at  $r = 10^3$ , we have  $\Delta\eta \simeq 2000$ . Therefore, the time duration  $\Delta\eta$  is increasing with  $r$ . This result shows that the time duration seems to be dependent mainly on the size  $r$  (or optical depth  $\tau$ ) of the halo, regardless the initial time duration  $\Delta\eta = \eta_0$ .

The bottom two panels of Figure 8 are for flash sources with original time duration  $\Delta\eta = \eta_0 = 100$  (left) and 500 (right), and  $r = 10^3$ . The light curves of the bottom two panels  $f_{100}(\eta)$  (left) and  $f_{500}(\eta)$  (right) of Figure 8 are about the same, i.e.  $f_{500}(\eta) \simeq 5f_{100}(\eta)$ . Although the two flash sources have very different time durations at  $r = 0$ , the two light curves and time duration actually are about the same. The coefficient 5 is due to the total number of photons given by the flash  $\eta_0 = 500$  is 5 times larger than that of  $\eta_0 = 100$ . This result shows again that the time duration is only dependent on the size  $r$ , regardless the original time duration.

This feature indicates that the spatial transfer of a flash essentially is a diffusion process. As mentioned in §3, the spatial transfer of resonant photons cannot be described as a purely Brownian diffusion process, by which the time duration  $\Delta\eta$  should increase with  $r^2$  or  $\tau^2$ . On the other hand, if the spatial transfer of a photon can be, in average, described by constant speed, the time duration  $\Delta\eta$  of a flash should be, in average, equal to the original one. However, Figure 8 shows that the time duration  $\Delta\eta$  is roughly proportional to  $r$ , and independent of the initial time duration. Therefore, the spatial transfer of resonant photons essentially is still a diffusion process.

### 4.3. Delayed emission line of stored photons

The effect of trapping and storing photons in an optical thick halo can be more clearly revealed with a flash source. Let us consider a flash source with a continuum spectrum, which is described by equation (18), but take  $S_0\phi_s(x) = 1$ . The time evolutions of  $j$  and  $f$  for  $\eta_0 = 50$  at  $r = 10^2$  are presented in Figure 9, in which we take the time to be  $\eta = 200, 300$  and  $500$ .

The top panels show the evolution of the mean intensity  $j$  in the halo. In an early time  $\eta = 200$ , there are photons in the central range  $|x| < 4$  as well as in wings  $|x| > 4$ . At later time  $\eta = 300$ , wing photons disappear, because all wing photons from the flash source have already escaped from the  $r$  halo. At time  $\eta = 500$ , the mean intensity  $j$  of  $|x| < 4$  is still about the same as  $j$  at  $\eta = 300$ . The flat plateau of  $j$  is shown in all time. Therefore, the local thermalized photons are stored in the halo at least from time  $\eta = 200$  to  $500$ , which is much longer than the  $\eta_0 = 50$ .

The evolution of flux  $f$  given by the bottom panels of Figure 9 is more interesting. At the time  $\eta = 200$ , the flux shows a typical absorption line at  $\nu_0$ . However, at  $\eta = 300$ , the flux  $f$  becomes a typical emission line with two peak profile. At time  $\eta = 500$ ,  $f$  is still a two peak emission line. The flux of the emission at  $\eta = 500$  is as strong as that at  $\eta = 300$ . Its light curve is similar to same as the top left panel of Figure 8. Note that Figure 8 is for a source of emission line, while Figure 9 is for a continuum spectrum. The similarity of the light curves of Figures 8 and 9 is again due to the local thermalization and the diffusion in physical space, both of which lead to the initial frequency spectrum and the time dependence of the photon sources being forgotten.

The emission at  $\eta > 300$  is a delayed emission, as the flash of source has already ceased. The photons of the delayed emission is provided by the  $|x| < 4$  photons stored in the halo  $r < 10^2$ . The time duration of the delayed emission is about the same as the time scale of

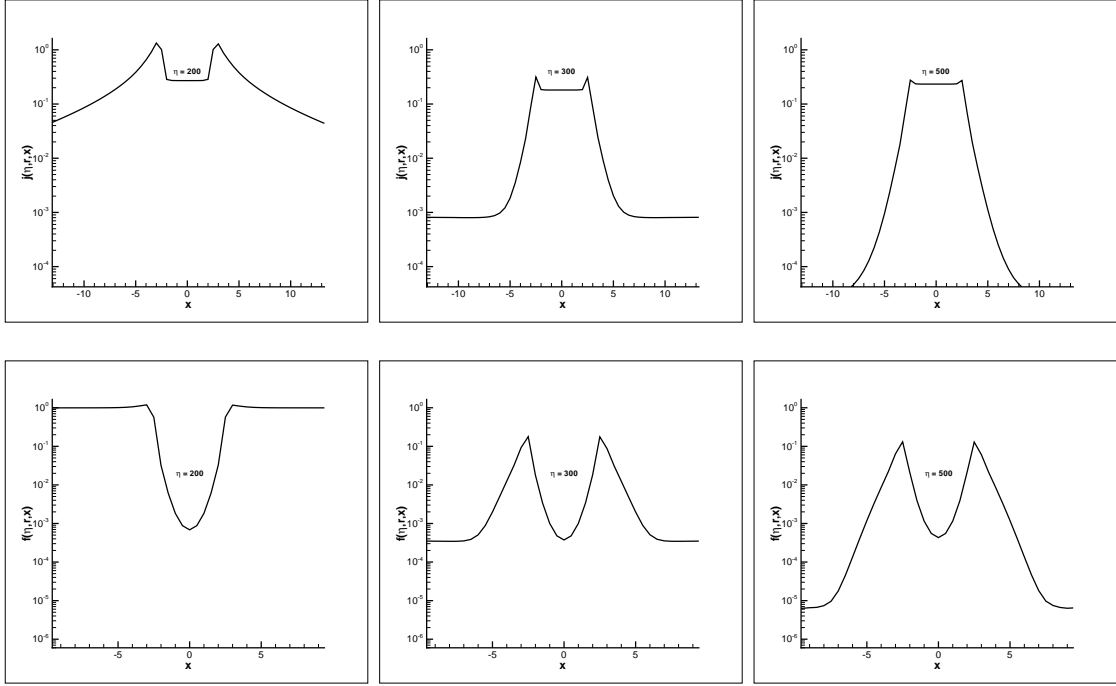


Fig. 9.— Profiles of  $j(\eta, r, x)$  (top) and  $f(\eta, r, x)$  (bottom) at  $r = 10^2$  when a flash source eq.(18) with  $\eta_0 = 50$  and  $S_0\phi_s(x) = 1$ . The time is  $\eta = 200$  (left), 300 (middle) and 500 (right).

the decaying phase of Figure 8. Therefore, it is also proportional to  $r$ , regardless the original time duration. Thus, at large  $r$ , a flash with a continuant spectrum and very short original time duration  $\eta_0$  can produce a two peak emission. Figure 9 shows also that at  $r = 10^2$  the luminosity of the peaks of the emission line at  $\eta = 300$  and 500 are about 1/10 of the continuum in that frequency range.

## 5. Discussions and Conclusions

The resonant scattering made the transfers of resonant photons in physical space and frequency space to be coupled from each other. It leads to the time scale  $\eta$  of the spatial transfer of the resonant photons in the halo with optical depth  $\tau \gg 1$  being much faster than a purely Brownian diffusion process requiring  $\eta \propto \tau^2$ . However, essentially it is still a diffusion process, which can be approximately described by  $\eta \propto \tau^{1/H}$ , with the index  $H$  less than but very close to 1. It is possible, if we consider the single longest excursion playing the role of a long-range dependence, that this diffusion process has a positive correlation, or

is a fractal Brownian diffusion (e.g. Beran 1994).

The number of photons basically is conserved. Thus, an optically thick halo is a store of photons with frequency  $\sim \nu_0$ . The time scale of the store is the same as the time scale of the above-mentioned diffusion, i.e. approximately proportional to the optical depth  $\tau$ . Moreover, the stored photons are always in the state of local Boltzmann distribution, even when the mean intensity is highly time-dependent. The initial conditions are forgotten in the process of approaching the local thermal equilibrium. The local Boltzmann distribution is independent of the frequency spectrum and time-dependence of the source.

These basic properties yield the following features of Ly $\alpha$  photons emergent from an optical thick halo.

1. At a given  $r$ , the profile of the two peaks of the flux is time-independent, and also independent of the initial profile of the photons. Therefore, it is impossible to estimate the line profile of the source from the profile of the flux emergent from an optical thick halo.
2. The frequencies  $|x_{\pm}|$  of the two peaks of the flux is not less than about 2. This would be useful to estimate the kinetic temperature of the neutral hydrogen atoms.
3. The resonant scattering makes the flux of the red damping wing very different from that of the DLA model. The flux is non-zero at frequency  $\nu_0$  or  $x = 0$ . These results would be useful to discriminate the DLA model with models which consider the effect of resonant scattering.
4. The light curves of the delayed emission of Ly $\alpha$  photons from a flash source is mainly determined by the optical depth of the halos, since the halo generally is transparent for high energy photons. A comparison between the light curves of Ly $\alpha$  photons and high energy photons would be useful to detect the halo.

For halos with large optical depth, the parameter  $\gamma$  is small even at high redshift. When  $\gamma \sim 10^{-5}$ , the effect of cosmic expansion on photon evolution in the frequency space actually is negligible. All solutions  $f(\eta, r, x)$  given in this paper are almost independent of the Hubble expansion. The effect of  $\gamma$  would be important if the considered time scale  $\eta$  of  $f$  is comparable with that of the Hubble expansion.

This work is supported in part by NSF grant AST-0506734 and ARO grant W911NF-08-1-0520.

## A. Numerical algorithm

To solve equations (9) and (10) as a system, our computational domain is  $(r, x) \in [0, r_{max}] \times [x_{left}, x_{right}]$ , where  $r_{max}$ ,  $x_{left}$  and  $x_{right}$  are chosen such that the solution vanishes to zero outside the boundaries. In the following, we describe numerical techniques involved in our algorithm, including approximations to the spatial derivatives, integrals in the frequency domain, numerical boundary condition and time evolution.

### A.1. The WENO algorithm: approximations to the spatial derivatives

The spatial derivative terms in equations (9) and (10) are approximated by a fifth order finite difference WENO scheme.

We first give the WENO reconstruction procedure in approximating  $\frac{\partial j}{\partial x}$ ,

$$\frac{\partial j(\eta^n, r_i, x_j)}{\partial x} \approx \frac{1}{\Delta x} (\hat{h}_{j+1/2} - \hat{h}_{j-1/2}), \quad (\text{A1})$$

with fixed  $\eta = \eta^n$  and  $r = r_i$ . The numerical flux  $\hat{h}_{j+1/2}$  is obtained by the fifth order WENO approximation in an upwind fashion, because the wind direction is fixed. Denote

$$h_j = j(\eta^n, r_i, x_j), \quad j = -2, -1, \dots, N+3 \quad (\text{A2})$$

with fixed  $n$  and  $i$ . The numerical flux from the WENO procedure is obtained by

$$\hat{h}_{j+1/2} = \omega_1 \hat{h}_{j+1/2}^{(1)} + \omega_2 \hat{h}_{j+1/2}^{(2)} + \omega_3 \hat{h}_{j+1/2}^{(3)}, \quad (\text{A3})$$

where  $\hat{h}_{j+1/2}^{(m)}$  are the three third order fluxes on three different stencils given by

$$\begin{aligned} \hat{h}_{j+1/2}^{(1)} &= -\frac{1}{6}h_{j-1} + \frac{5}{6}h_j + \frac{1}{3}h_{j+1}, \\ \hat{h}_{j+1/2}^{(2)} &= \frac{1}{3}h_j + \frac{5}{6}h_{j+1} - \frac{1}{6}h_{j+2}, \\ \hat{h}_{j+1/2}^{(3)} &= \frac{11}{6}h_{j+1} - \frac{7}{6}h_{j+2} + \frac{1}{3}h_{j+3}, \end{aligned}$$

and the nonlinear weights  $\omega_m$  are given by,

$$\omega_m = \frac{\check{\omega}_m}{\sum_{l=1}^3 \check{\omega}_l}, \quad \check{\omega}_l = \frac{\gamma_l}{(\epsilon + \beta_l)^2}, \quad (\text{A4})$$

where  $\epsilon$  is a parameter to avoid the denominator to become zero and is taken as  $\epsilon = 10^{-8}$ . The linear weights  $\gamma_l$  are given by

$$\gamma_1 = \frac{3}{10}, \quad \gamma_2 = \frac{3}{5}, \quad \gamma_3 = \frac{1}{10}, \quad (\text{A5})$$

and the smoothness indicators  $\beta_l$  are given by,

$$\begin{aligned} \beta_1 &= \frac{13}{12}(h_{j-1} - 2h_j + h_{j+1})^2 + \frac{1}{4}(h_{j-1} - 4h_j + 3h_{j+1})^2, \\ \beta_2 &= \frac{13}{12}(h_j - 2h_{j+1} + h_{j+2})^2 + \frac{1}{4}(h_j - h_{j+2})^2, \\ \beta_3 &= \frac{13}{12}(h_{j+1} - 2h_{j+2} + h_{j+3})^2 + \frac{1}{4}(3h_{j+1} - 4h_{j+2} + h_{j+3})^2. \end{aligned}$$

To approximate the  $r$ -derivatives in the system of equations (9) and (10), we need to perform the WENO procedure based on a characteristic decomposition. We write the left hand side of equations (9) and (10) as

$$\mathbf{u}_t + A\mathbf{u}_r \quad (\text{A6})$$

where  $\mathbf{u} = (j, f)^T$  and

$$A = \begin{pmatrix} 0 & 1 \\ \frac{1}{3} & 0 \end{pmatrix}$$

is a constant matrix. To perform the characteristic decomposition, we first compute the eigenvalues, the right eigenvectors, and the left eigenvectors of  $A$  and denote them by,  $\Lambda$ ,  $R$  and  $R^{-1}$ . We then project  $\mathbf{u}$  to the local characteristic fields  $\mathbf{v}$  with  $\mathbf{v} = R^{-1}\mathbf{u}$ . Now  $\mathbf{u}_t + A\mathbf{u}_r$  of the original system is decoupled as two independent equations as  $\mathbf{v}_t + \Lambda\mathbf{v}_r$ . We approximate the derivative  $\mathbf{v}_r$  component by component, each with the correct upwind direction, with the WENO reconstruction procedure similar to the procedure described above for  $\frac{\partial j}{\partial x}$ . In the end, we transform  $\mathbf{v}_r$  back to the physical space by  $\mathbf{u}_r = R\mathbf{v}_r$ . We refer the readers to Cockburn et al. 1998 for more implementation details.

## A.2. Adaptive mesh procedure for non-uniform grid

A fifth order conservative finite difference WENO scheme can only be applied to a uniform grid or a smoothly varying grid. A smooth transformation,

$$\xi = \xi(r) \quad (\text{A7})$$

gives us a uniform grid in a new variable  $\xi$ . In this case  $\xi$  is sufficiently smooth, i.e., it has as many derivatives as the order of accuracy of the scheme. Therefore the left hand side of the (9) and (10) as

$$\mathbf{u}_t + A\mathbf{u}_r \tag{A8}$$

where  $\mathbf{u} = (j, f)^T$  and

$$A = \begin{pmatrix} 0 & 1 \\ \frac{1}{3} & 0 \end{pmatrix}$$

is transformed to

$$\mathbf{u}_t + A\xi_r\mathbf{u}_\xi \tag{A9}$$

and the WENO derivative approximation is now applied to  $\mathbf{u}_\xi$ .

## REFERENCES

- Adams, T.F. 1972, ApJ, 174, 439
- Ahn, S.-H., Lee, H.W., & Lee, H. M. 2002, ApJ, 567, 922
- Avery, L.W., & House, L.L. 1968, ApJ, 152, 493
- Beran, J. 1994, Statistics for Long-Memory Processes, Chapman & Hall.
- Cantalupo, S., Porciani, C., Lilly, S.J. & Miniati, F. 2005, ApJ, 628, 61
- Carrillo, J.A., Gamba, I.M., Majorana, A. & Shu, C.-W. 2003, Journal of Computational Physics, 184, 498
- Carrillo, J.A., Gamba, I.M., Majorana, A. & Shu, C.-W. 2006, Journal of Computational Physics, 214, 55
- Cen, R. 2006, ApJ, 648, 47
- Cockburn, B., Johnson, C., Shu, C-W. & Tadmor, E. 1998, Lecture Notes in Mathematics, 1697, 450
- Dijkstra, M., Haiman, Z. & Spaans, M. 2006, ApJ, 649, 14
- Fang, L.Z., 2009, Inter. J. Mod. Phys. D18, 1943
- Field, G.B., 1958, Proc. IRE, 46, 240
- Field, G.B. 1959, ApJ, 129, 551.

- Haiman, Z., & Cen, R. 2005, *ApJ*, 623, 627
- Harrington, J.P. 1973, *MNRAS*, 162, 43
- Heney, L.G. 1941, *Proc. Nat. Acad. Sci.* 26, 50
- Hummer, D.G. 1962, *MNRAS*, 125, 21
- Hummer, D.G. 1965, *Mem. R. astr. Soc.*, 70, 1
- Hummer, D.G. 1969, *MNRAS*, 145, 95
- Jiang, G. & Shu, C.-W. 1996, *J. Comput. Phys.*, 126, 202
- Lee, J.S. 1974, *ApJ*, 192, 465
- Liu, J.-R., Qiu, J.-M., Feng, L.-L., Shu, C.-W. & Fang, L.-Z. 2007, *ApJ*, 663, 1
- McQuinn, M., Hernquist, L., Zaldarriaga, M. & Dutta, S. 2007, *MNRAS*, 381, 75
- Miralda-Escude, J. & Rees, M.J. 1998, *ApJ*, 497, 21
- Miralda-Escude, J. 1998, *ApJ*, 501, 15
- Neufeld, D. 1990, *ApJ*, 350, 216
- Osterbrock, D.E. 1962, *ApJ*, 135, 195
- Qiu, J.-M., Feng, L.-L., Shu, C.-W. & Fang, L.-Z. 2006, *New Astronomy*, 12, 1
- Qiu, J.-M., Feng, L.-L., Shu, C.-W. & Fang, L.-Z. 2007, *New Astronomy*, 12, 398
- Qiu, J.-M., Shu, C.-W., Liu, J.-R. & Fang, L.-Z. 2008, *New Astronomy*, 13, 1
- Roy, I., Qiu J.-M., Shu C.-W. & Fang L.-Z., (2009a) *New Astronomy* 14, 513
- Roy, I. Xu, W., Qiu J.-M., Shu C.-W. & Fang L.-Z., (2009b) *ApJ*, 694, 1121
- Roy, I. Xu, W., Qiu J.-M., Shu C.-W. & Fang L.-Z., (2009c) *ApJ*, 703, 1992
- Salvaterra, R., et al. 2009, *Nature*, 461, 1258
- Spitzer, L. & Greenstein, J.L. 1951, *ApJ*, 114, 407
- Tanvir, N.R. et al. 2009, *Nature*, 461, 1254
- Tasitsiomi, A. 2006, *ApJ*, 645, 792

Totani, T. et al. 2006, Publ. Astron. Soc. Japan. 58, 485

Unno, W. 1955, Publ. Astron. Soc. Japan. 7, 81

Verhamme, A., Schaerer, D. & Maselli, A. 2006, AA

Vreeswijk, P.M. et al. 2004, AA, 419, 927

Wouthuysen, S. A. 1952, AJ, 57, 31

Zheng, Z. & Miralda-Escude, J., 2002, ApJ, 578, 33